RSC Advances

ROYAL SOCIETY OF CHEMISTRY

www.rsc.org/advances

In-situ Sodium Chloride Template Synthesis of Cobalt Oxide Hollow Octahedrons for Lithium-ion Batteries

Fei Wang*, Danfei Cheng, Wengang Wang, Yuting Wang, Mingshu Zhao, Shengchun Yang, Xuegang Lu and Xiaoping Song

School of Science, Key Laboratory of Shaanxi for Advanced Functional Materials and Mesoscopic Physics, State Key Laboratory for Mechanical Behavior of Materials, Xi'an Jiaotong University, Xi'an 710049, ShaanXi, People's Republic of China

Abstract

A novel template synthesis route is developed to synthesize cobalt oxide hollow octahedrons. The sodium chloride templates are formed in-situ in the reaction system by controlling the supersaturation of sodium chloride in the N,N-Dimethylformamide solution. Transmission electron microscopy indicates that the porous shells of hollow octahedrons are composed of ultra small particles. Electrochemical tests show that the discharge capacity of the cobalt oxide hollow octahedrons is about 965 mAh g^{-1} after 30 cycles at 0.2 C.

Keywords: Cobalt oxide; Octahedron; Hollow structure; Anode; Lithium-ion battery

1. Introduction

Lithium-ion batteries (LIBs) are the predominant power source for portable electronics at present due to their high energy density and long cycle life, etc. [1] However, further applications of LIBs in

Tel: +86 29 82663034; Fax: +86 29 82665995; E-mail address: feiwang@mail.xjtu.edu.cn (F. Wang)

high energy areas, such as electric vehicles (EVs) and large-scale energy storage systems, are still restricted. Therefore, with the growing demand for higher capacity and safety, numerous efforts have been made to develop alternative high-performance electrode materials for next-generation LIBs. [2-3] Recently, nano-sized transition metal oxides have been widely investigated as promising anodes for LIBs due to their higher theoretical capacities than conventional graphite materials (<372 mAh g^{-1}).[3-14] For example, the theoretical capacity of Co_3O_4 reach to 892 mAh g^{-1}. However, the severe volume variation that occurs during repeated lithiation/delithiation processes is a big challenge to obtain excellent cycling performance. [15-18] One of the effective strategies to alleviate these problems is to design hollow micro-/nanostructured electrode materials instead of conventional solid micro-/nanostructures.[19-22] The larger specific surface area of the hollow structures can lead to increased electrode-electrolyte contact area and more lithium storage sites. The thin shells of them can significantly reduce the diffusion paths for both Li ions and electrons, leading to the faster reaction kinetics at the electrode surface. Moreover, the hollow interior can provide additional free space to alleviate the structural strain associated with repeated lithium uptake/removal processes and thus lead to improved cycling performance.

The general route for preparing hollow nanostructures is based on the controlled deposition of the designed materials onto removable templates. [23, 24] The templates, such as polystyrene [25], silica [26] and cuprous oxide [27], are prepared in advance and removed via chemical etching or thermal decomposition after deposition. Therefore, these method are usually tedious, costly and instability because of the multistep procedures involving template preparation, shell deposition and template removal. In this paper, we present a facile template approach to synthesize uniform Co_3O_4 hollow octahedrons. The used NaCl templates are formed in situ during reaction process and can be easily

removed by distilled water. The obtained Co_3O_4 hollow octahedrons exhibit high reversible capacity and superior cycling performance.

2. Experimental

In a typical synthesis, 0.1 g poly-(vinyl pyrrolidone) (PVP), 1.0 g poly(ethylene glycol) (PEG), 0.71 g $CoCl_2 \cdot 6H_2O$ and 0.3 g NaCl were added to a three-neck round-bottom flask containing 45 ml N, N-dimethylformamide (DMF). The mixture was maintained at 40 ^oC, followed by the addition of 15 ml DMF solution containing 0.16 g sodium borohydride ($NaBH_4$) with stirring. The final solution was then kept at 40 °C for 1 h. After the reaction, the resulting suspension was washed and NaCl templates were simultaneously removed by distilled water and ethanol. The precipitate was separated from the mixture by centrifugation at 5000 rpm for 2 min and dried at 60 °C for 12 h. Finally, the dried powders were heat-treated in air for 2 h at 500 ^oC.

The structure and morphology of the products were characterized by X-ray diffraction (XRD, Bruke D8-Advance, Cu-Kα, λ = 0.15406 nm), field emission scanning electron microscope (FESEM, JEOL JSM-7100F) and transmission electron microscopy (TEM, JEOL JEM-2100). Energy dispersive X-ray (EDX) analysis was obtained with an Oxford INCA detector installed on the FESEM.

Electrochemical properties of Co_3O_4 hollow octahedrons were tested using two-electrode Swagelok cells with lithium metal as the counter and reference electrodes. The working electrodes consisted of 80 wt.% active materials (Co_3O_4), 10 wt.% conductive materials (acetylene black), and 10 wt.% binder (polyvinylidene fluoride, PVDF). The electrolyte was 1 M $LiPF_6$ in a mixture of 50 vol.% ethylene carbonate (EC) and 50 vol.% diethylene carbonate (DEC). Test cells were assembled in argon filled glove box (Mikrouna Super 1220/750). The galvanostatical charge-discharge measurement was carried out on Arbin BT2000 battery testing system in the voltage range of 0.02 V-3.0 V (vs. Li/Li+). The

cyclic voltammograms (CV) were tested on Ametek VMC-4 electrochemical testing system at a scan rate of 0.5 mV s^{-1} between 0 V and 3.0 V (vs. Li/Li^+).

3. Results and discussion

Figure 1 shows the electron microscopic data of the reaction products only briefly washed by ethanol in order to maintain the NaCl templates. All particles in the SEM images show the typical solid octahedron morphology with the size range of 2-4 μm. The inset pattern of Figure 1a shows the XRD analysis of the solid octahedrons. All diffraction peaks in it can be indexed to cubic NaCl structure (JCPDS No. 05-0628). The formation of NaCl crystals is ascribed to the limited solubility of NaCl in DMF solution. Thus, the NaCl concentration plays an important role to obtain the octahedral NaCl template. Only when the NaCl concentration over a certain range of its saturated solubility, the octahedral NaCl templates can be well formed. Thus, the additional NaCl (0.3 g) is needed besides the NaCl resultant from the chemical reaction (equation 1). Otherwise, the products are the dispersive spherical nanoparticles (Figure S1). From the EDX spectrum (the inset pattern of Figure 1b) we can see that Co and O elements also exist besides Na and Cl. The absence of the cobalt oxide diffraction peaks in the XRD pattern should be attributed to the poor crystallinity of the cobalt oxide. Thus, the diffraction peaks of cobalt oxide are submerged in the sodium chloride diffraction peaks due to the striking contrast of the diffraction intensity. The formation of the cobalt oxide can be described as two-step reaction processes, which are the reduction of Co (II) ions to metallic Co (0) by $NaBH_4$ and the further oxidation of metallic Co to cobalt oxide, as shown in equations 1-2.

$$CoCl_2 + NaBH_4 \rightarrow Co + H_2 + NaCl + BCl_3 \quad (1)$$

$$Co + O_2 \rightarrow Co_3O_4 \quad (2)$$

The formation of the solid octahedrons can be schematically illustrated by Figure 2. At the first stage,

the Co_3O_4 small crystallites were deposited on the surface of the in situ formed NaCl crystals, which act as the template for the formation of the octahedrons. At the stage II, the deposited Co_3O_4 small crystallites would attach to each other because of the Oswald ripening occurring in organic solvent, which leads to the formation of shell layer on the surface of NaCl crystals.

When the solid octahedron particles were washed with distilled water, the NaCl templates were removed while the cobalt oxide can be reserved due to the different water solubility between ionic compounds and oxides (the stage III of Figure 2). EDX pattern (the inset pattern of Figure 3b) indicates that there are only Co and O elements existing. SEM images (Figure 3a, b) show that the octahedron morphology has been well maintained after the removing of the NaCl templates. The hollow structure can be clearly observed in the TEM image of an individual Co_3O_4 octahedron (Figure 3c). Comparing with the solid octahedrons with NaCl templates, the hollow octahedrons have an obvious shrinkage and the size of the octahedrons is reduced to the range of 1-2 μm. The rough shells composed of the interlaced nanosheets (Figure 3c, d) should be ascribed to the shrink of the shell materials during the removing of the NaCl templates.

To improve the structure stability and the lithium storage properties of cobalt oxide, the hollow octahedrons have been heat-treated at 500 ^oC for 2 h before the testing as anode materials for LIBs. Comparing with the untreated hollow octahedrons, it is similar in both octahedron morphology and size after the heat treatment (Figure 4a). However, from the TEM image (Figure 4b) we can see clearly that obvious changes have taken place in the shell. After the heat treatment, the interlaced nanosheets have transformed into porous structure composed of the small particles about 5 nm due to the atom diffusion in high temperature. The corresponding SEAD characterization shows the ring-like diffraction pattern

(Figure 4c), which suggests that the hollow octahedrons are poor crystallinity even after the heat treatment at 500 ^{o}C. All the diffraction rings could be assigned to the spinel-type Co_3O_4 (JCPDS No. 42-1267), which is consistent with the XRD analysis (the inset pattern of Figure 4a). The size of the particles and holes can be observed more clearly in high-resolution TEM image (Figure 4d). The interplanar spacing marked in it is about 0.24 and 0.47 nm, corresponding to the (311) and (111) plane of the cubic Co_3O_4, respectively.

The electrochemical reaction processes are investigated by cyclic voltammograms. Fig. 5a shows the CV curves of the Co_3O_4 hollow octahedrons heat treated at 500 ^{o}C. During the first cathodic scan, only one broad peak near 0.5 V could be observed. Compared to the initial cycle, a decrease of peak intensity and a shift of the potential to the positive direction are revealed in the subsequent cycles. This cathodic peak corresponds to a multistep electrochemical reaction, which is generally attributed to the reduction of Co (III) to Co (II) and metal Co. [28] In the anodic scans, one peak at about 2.18 V is recorded, which are ascribed to the reversible oxidation of metal Co to cobalt oxide. Except for the first cycle, the following CV curves are similar, which demonstrate the good cycle stability of Co_3O_4 hollow octahedrons during the discharge-charge cycles. The electrochemical reaction of Li with Co_3O_4 can be expressed as equation 3. [29-31]

$$Co_3O_4 + 8Li^+ + 8e^- \leftrightarrow 4Li_2O + 3Co \quad (3)$$

Figure 5b shows the cycling performance and coulomb efficiency of the Co_3O_4 hollow octahedrons heat treated at 500 ^{o}C. The initial discharge and charge capacities are 2058 and 1213 mAh g^{-1}, respectively. The initial irreversible capacities are mainly ascribed to the decomposition of the electrolyte and the formation of the SEI layer, [28, 32] which are significantly influenced by the specific surface area of the electrode materials. Due to the large specific surface area, the coulomb

efficiency of the Co_3O_4 hollow octahedrons in the first cycle is only 58.9%. However, the coulomb efficiencies are increased rapidly and stabilized above 98% after 5 cycles. Except the first cycle, no obvious capacity fade is found within 30 cycles and the discharge capacity at 30th cycle can be maintained at 965 mAh g^{-1}. As a comparison, the discharge capacity of the Co_3O_4 spherical nanoparticles (Figure S1) is only 672 mAh g^{-1} at 30th cycle, as shown in Figure 5d. The rate capability of Co_3O_4 hollow octahedrons heat treated at 500 ^oC is studied and presented in Figure 5c. From the rate capability curve we can see that the capacity and cyclability have a notable deterioration at 1.0 C, which should be ascribed to the poor crystallinity of the Co_3O_4 hollow octahedrons. The abundant crystallite boundaries is disadvantageous to the charge transfer during lithiation/delithiation processes. Even so, the discharge capacity can return to about 1000 mAh g^{-1} when the current density turns back to 0.2 C, which indicate that the hollow structure can be kept well even after charge-discharge at high current density. The superior cycling performance of the Co_3O_4 octahedrons should be attributed to its hollow structure with porous shells composed of ultra small particles, which is beneficial for accommodating the strain induced by the severe volume variations during Li^+ insertion and extraction.

4. Conclusions

The Co_3O_4 hollow octahedrons are successfully synthesized by a simple in-situ NaCl template synthesis route. The porous shells of the Co_3O_4 hollow octahedrons are composed of ultra small particles, which is beneficial for accommodating the strain induced by the severe volume variations during Li^+ insertion and extraction. Electrochemical studies indicate that the obtained Co_3O_4 hollow octahedrons exhibit high capacity and superior cycling performance. The current in-situ NaCl template method is also appropriate to synthesize other hollow metal oxide anode materials.

Acknowledgements

This work was supported by National Natural Science Foundation of China (51172178 and 51302214), Program for Key Science and Technology Innovative Research Team of Shaanxi Province (2013KCT-05) and Fundamental Research Funds for the Central Universities.

References

[1] M. Armand, J.M. Tarascon, Nature 451 (2008) 652-657.

[2] Y. Idota, T. Kubota, A. Matsufuji, Y. Maekawa, T. Miyasaka, Science 276 (1997) 1395-1397.

[3] P. Poizot, S. Laruelle, S. Grugeon, L. Dupont, J.M. Tarascon, Nature 407 (2000) 496-499.

[4] K.M. Shaju, F. Jiao, A. Débart, P.G. Bruce, Phys. Chem. Chem. Phys. 9 (2007) 1837-1842.

[5] X.W. Lou, D. Deng, J.Y. Lee, L.A. Archer, J. Mater. Chem. 18 (2008) 4397-4401.

[6] F.M. Zhang, B.Y. Geng, Y.J. Guo, Chem. Eur. J. 15 (2009) 6169-6174.

[7] L. Tian, H.L. Zou, J.X. Fu, X.F. Yang, Y. Wang, H.L. Guo, X.H. Fu, C.L. Liang, M.M. Wu, P.K. Shen, Q.M. Gao, Adv. Funct. Mater. 20 (2010) 617-623.

[8] J. Liu, H. Xia, L. Lu, D.F. Xue, J. Mater. Chem. 20 (2010) 1506-1510.

[9] X.Y. Xue, S. Yuan, L.L. Xing, Z.H. Chen, B. He, Y.J. Chen, Chem. Commun. 47 (2011) 4718-4720.

[10] X. Wang, H. Guan, S.M. Chen, H.Q. Li, T.Y. Zhai, D.M. Tang, Y. Bando, D. Golberg, Chem. Commun. 47 (2011) 12280-12282.

[11] Y. Sun, X.Y. Feng, C.H. Chen, J. Power Sources 196 (2011) 784-787.

[12] S.L. Xiong, J.S. Chen, X.W. Lou, H.C. Zeng, Adv. Funct. Mater. 22 (2012) 861-871.

[13] F. Wang, C.C. Lu, Y.F. Qin, C.C. Liang, M.S. Zhao, S.C. Yang, Z.B. Sun, X.P. Song, J. Power Sources 235 (2013) 67-73.

[14] C.C. Liang, D.F. Cheng, S.J. Ding, P.F. Zhao, M.S. Zhao, X.P. Song, F. Wang, J. Power Sources 251 (2014) 351-356.

[15] D. Larcher, G. Sudant, J.B. Leriche, Y. Chabre, J.M. Tarascon, J. Electrochem. Soc. 149 (2002) A234-A241.

[16] Y. Yu, C.H. Chen, J.L. Shui, S. Xie, Angew. Chem. Int. Ed. 44 (2005) 7085-7089.

[17] X.W. Lou, D. Deng, J.Y. Lee, J. Feng, L.A. Archer, Adv. Mater. 20 (2008) 258-262.

[18] D. Fang, L.C. Li, W.L. Xu, G.Z. Li, G. Li, N.F. Wang, Z.P. Luo, J. Xu, L. Liu, C.L. Huang, C.W. Liang, Y.S. Ji, J. Mater. Chem. A 1 (2013) 13203-13208.

[19] T. He, D.R. Chen, X.L. Jiao, Y.Y. Xu, Y.X. Gu, Langmuir 20 (2004) 8404-8408.

[20] Y. Sun, X.Y. Feng, C.H. Chen, J. Power Sources 196 (2011) 784-787.

[21] N. Yan, L. Hu, Y. Li, Y. Wang, H. Zhong, X.Y. Hu, X.K. Kong, Q.W. Chen, J. Phys. Chem. C 116 (2012) 7227−7235.

[22] J.Y. Wang, N.L. Yang, H.J. Tang, Z.H. Dong, Q. Jin, M. Yang, D. Kisailus, H.J. Zhao, Z.Y. Tang, D. Wang, Angew. Chem. Int. Ed. 52 (2013) 6417-6420.

[23] Z.Y. Wang, L. Zhou, X.W. Lou, Adv. Mater. 24 (2012) 1903-1911.

[24] J. Hu, M. Chen, X.S. Fang, L.M. Wu, Chem. Soc. Rev. 40 (2011), 5472-5491.

[25] S.J. Ding, D.Y. Zhang, H.B. Wu, Z.C. Zhang, X.W. Lou, Nanoscale 4 (2012) 3651-3654.

[26] J.F. Ye, H.J. Zhang, R. Yang, X.G. Li, L.M. Qi, Small, 6 (2010) 296-306.

[27] Z.Y. Wang, D.Y. Luan, F.Y.C. Boey, X.W. Lou, J. Am. Chem. Soc. 133 (2011) 4738−4741.

[28] D. Larcher, G. Sudant, J.B. Leriche, Y. Chabre, J.M. Tarascon, J. Electrochem. Soc. 149 (2002) A234-A241.

[29] S. Laruelle, S. Grugeon, P. Poizot, M. Dolle, L. Dupont, J.M. Tarascon, J. Electrochem. Soc. 149

(2002) A627-A634.

[30] D. Barreca, M. Cruz-Yusta, A. Gasparotto, C. Maccato, J. Morales, A. Pozza, C. Sada, L. Sanchez, E. Tondello, J. Phys. Chem. C 114 (2010) 10054-10060.

[31] L. Tian, H.L. Zou, J.X. Fu, X.F. Yang, Y. Wang, H.L. Guo, X.H. Fu, C.L. Liang, M.W. Wu, P.K. Shen, Q.M. Gao, Adv. Funct. Mater. 20 (2010) 617-623.[32] P. Poizot, S. Laruelle, S. Grugeon, L. Dupont, J-M. Tarascon, J. Power Sources 97-98 (2001) 235-239.

Figure captions

Figure 1 (a, b) SEM images of the Co_3O_4 octahedrons with templates. The inset of (a) is the XRD pattern and the inset of (b) is the EDX pattern of the Co_3O_4 octahedrons with templates.

Figure 2 Schematic illustration of the formation of hollow Co_3O_4 octahedrons.

Figure 3 The representations of the untreated hollow Co_3O_4 octahedrons: (a, b) SEM images; (c) TEM image of an individual octahedron; (d) TEM image of the octahedron shell. The inset of (b) is the EDX pattern of the hollow Co_3O_4 octahedrons.

Figure 4 The representations of the hollow Co_3O_4 octahedrons heat-treated at 500 ^oC for 2 h: (a) SEM image; (b) TEM image of the octahedron shell; (c) the corresponding SAED pattern of (b); (d) HRTEM image of the octahedron shell. The inset of (a) is the XRD pattern of the hollow Co_3O_4 octahedrons heat-treated at 500 ^oC for 2 h.

Figure 5 Cyclic voltammogram curves (a), cycling performance (b) and rate capability (c) of the hollow Co_3O_4 octahedrons heat-treated at 500 ^oC for 2 h; (d) cycling performance of the Co_3O_4 spherical nanoparticles.

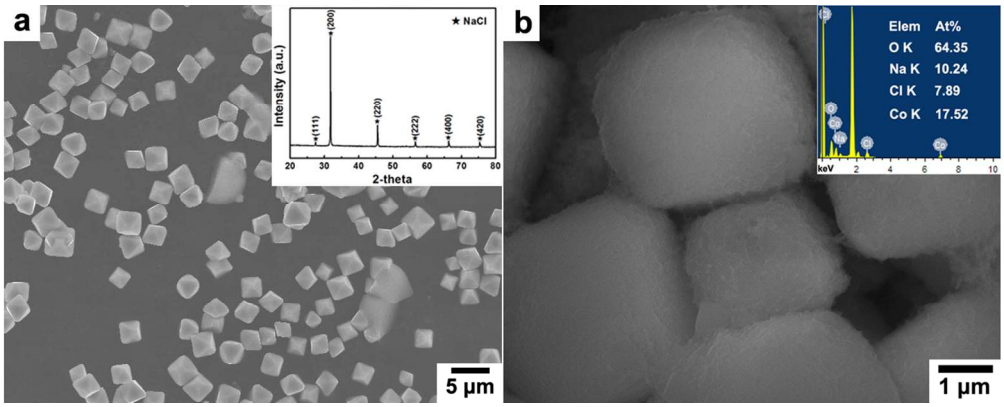

Figure 1
117x46mm (300 x 300 DPI)

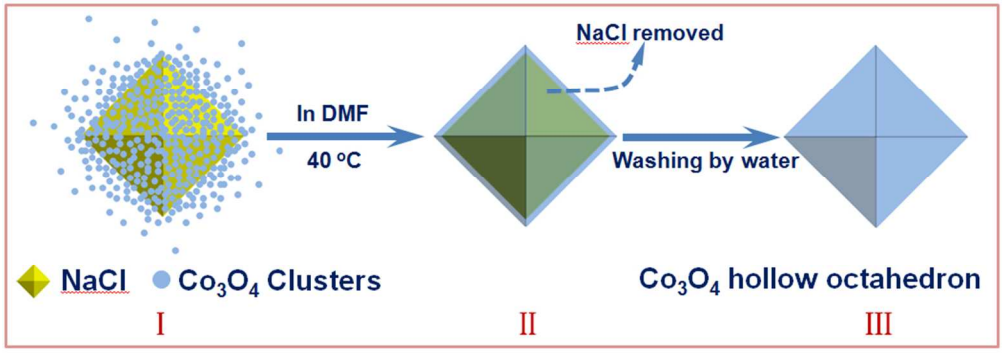

Figure 2
177x62mm (150 x 150 DPI)

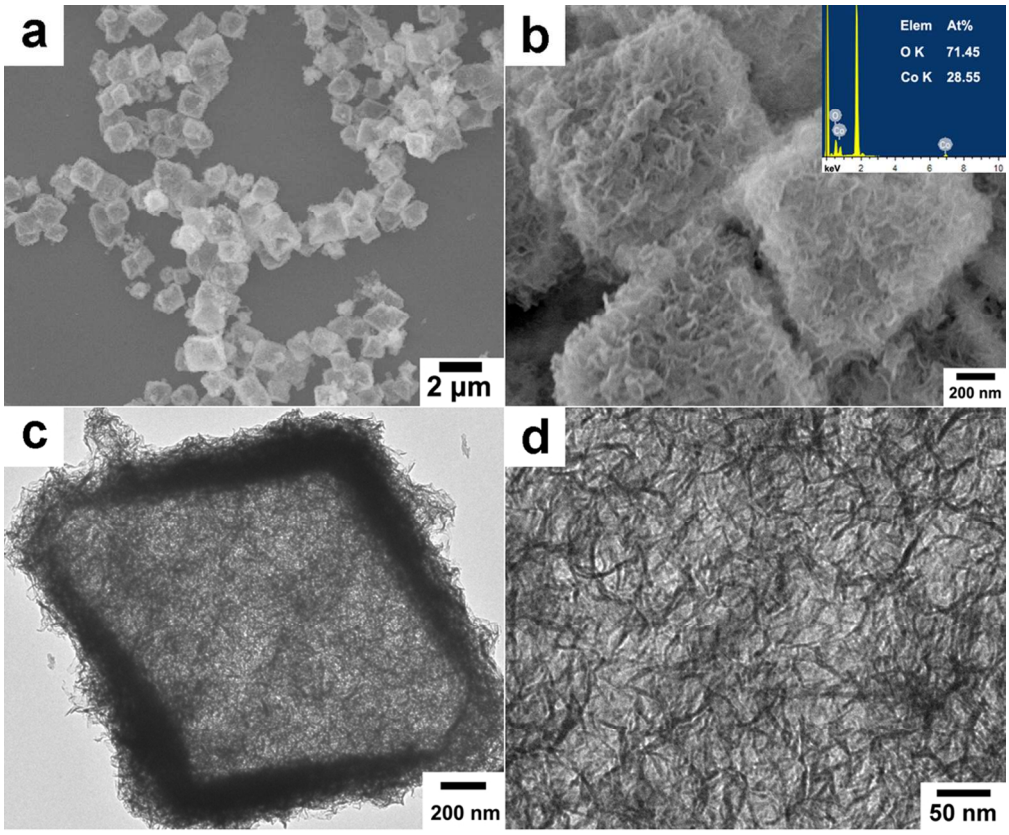

Figure 3
101x83mm (300 x 300 DPI)

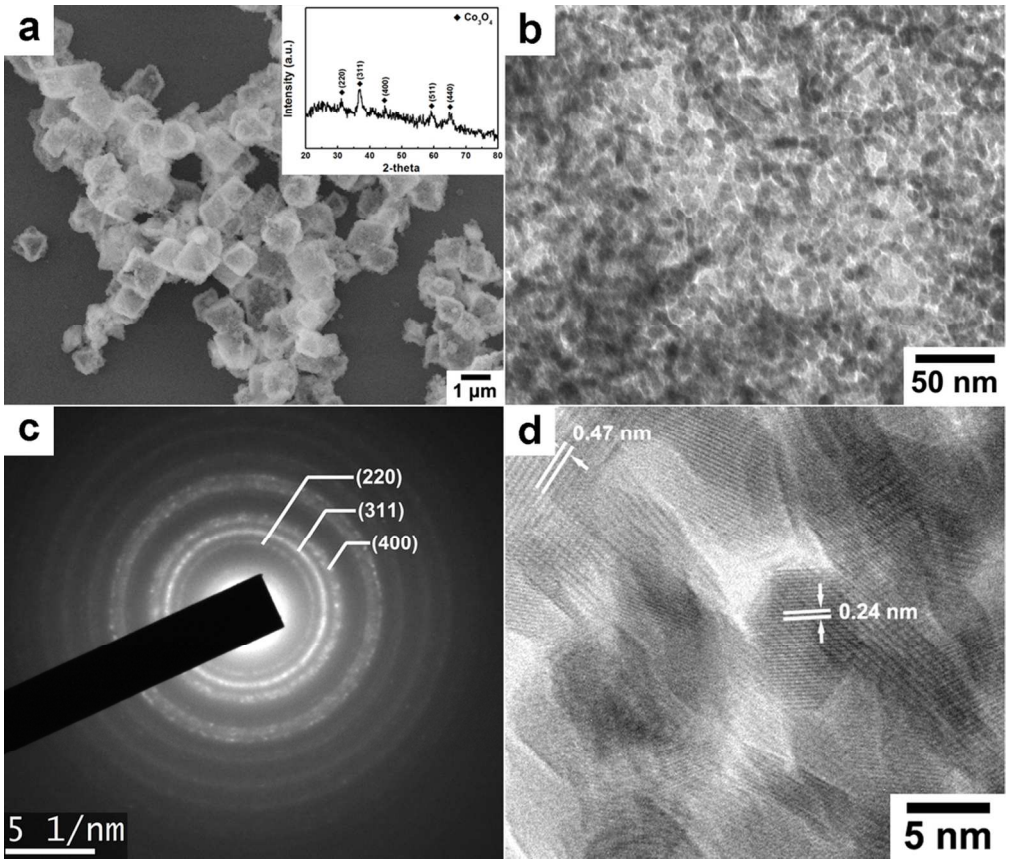

Figure 4
101x86mm (300 x 300 DPI)

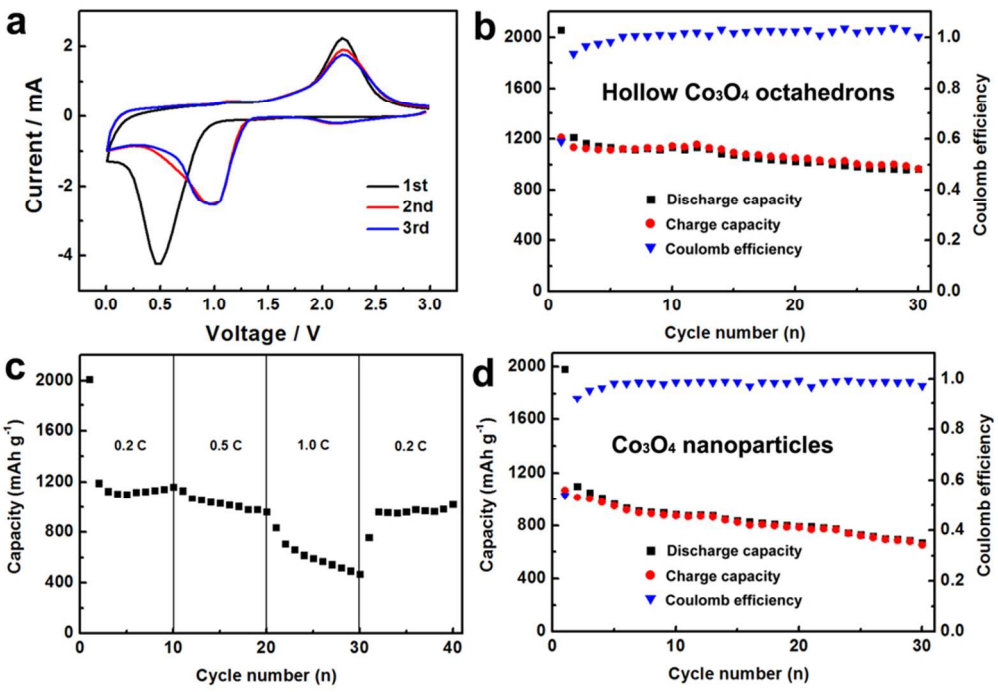

Figure 5
169x116mm (150 x 150 DPI)